

## RESEARCH ARTICLE

# Comparative fire-following-earthquake performance of code-compliant low-rise base-isolated structures

Huseyin Cilsalar 

Yozgat Bozok University, Department of Civil Engineering, Yozgat, Türkiye

## Article History

Received 17 February 2022

Accepted 11 June 2022

## Keywords

Post-earthquake fire

Seismic performance

Base isolation

Drift ratio

Steel frame

## Abstract

Seismic base isolation is an effective way of protecting structures against seismic loads and is very effective in terms of both collapse mitigation of structures and protection of non-structural elements under severe ground shaking. In this study, the structural demand of base-isolated three- and four-story steel moment-resisting frames is determined in case of a fire event followed by an earthquake, and compared with the results of fixed-base frames, which have similar geometry, load, and seismic hazard for a location in California. Four compartments are selected as possible locations for fire events in each building, and beams and columns in those compartments are exposed to a representative temperature increase in time, which includes a cooling phase as well. Maximum, minimum, and residual axial force, and moment demands on elements of the fire compartments, and drift demand of structural frames on the first and second floor, where the fire is assumed to occur, are determined and compared. Results are given in terms of parameters of three-parameter log-normal distribution, hence fragility curves can be constructed for each response considered in the study. Seismic isolation is effective in reducing both maximum and residual drift demand of the frames, and axial force in the beam element for each compartment considered. Fixed-base frames have 20% more maximum axial load on beams. Beam and column elements in the four-story configuration are under relatively more moments in case of a fire, while the performance of three-story frames depends on the location of the assumed fire.

## 1. Introduction

A fire event is a potential hazard for structural systems, especially if it is followed by severe ground shaking. Its damage might be more detrimental compared to an earthquake that might cause fire ignition inside the buildings. Due to altered properties of structural materials after fire exposition compared to ambient properties [1], structural systems may have higher demands after a fire if it is followed by an earthquake, and even there might be collapse although the structure had enough capacity to perform well during ground shaking. Hazard due to fire is not a threat only to buildings, due to spread, it is a danger to the community and its resilience. In case of a collapse in a fire event, the damaged building may block roads and delay responding to those in need. In history, there are some examples of such fire-following-earthquake events and how dangerous the consequences of these events are [2] for the building and the community.

Increased displacement and strength demands in structural elements are the possible cause of fire in a building due to damage to non-structural components. So, after a fire event, structural systems might undergo

some residual demand in the elements, which increases repair costs and may even require demolishing of the building due to increased cost. Protection of buildings against fire may help to achieve better performance in case of a fire, however, severe ground shaking can cause a malfunction in protection devices, and they may not perform as proposed. This will have a detrimental effect on structural performance in the event of a post-earthquake fire. So, structural demands should be reduced for the protection of buildings and devices inside, which can be achieved with seismic protective systems.

Isolation of structural system from the ground has prominent benefit in terms of protecting structures above the ground [3– 6]. Friction pendulum and rubber bearing are two main types that are used for the isolation of superstructure. Those elements provide stiffness and energy dissipation to the superstructure and are shown to be an effective way of mitigating seismic hazards for those structures constructed in earthquake-prone areas. Also, recent studies have shown that in addition to reducing demands on the superstructure, seismically isolated structures have relatively less seismic loss compared to fixed-base frames [7–10]. So, all these reasons make seismically isolated structures a promising technique for the protection of structures in highly seismic areas.

In this study, comparative post-earthquake fire performances of base-isolated three- and four-story structural steel frames are investigated. Structural drift and force demands in elements are evaluated. Frames considered in the study are designed for a location in California, which are lateral force resisting systems of a gravity framing system, and plans, loads, mass, etc. are the same for fixed and base-isolated frames. The only difference is that there is a base system on top of the isolator for those isolated frames. All structures are designed as per the requirement of ASCE/SEI 7-16 [11], and element connection and demands are determined and checked by the requirement of ANSI/AISC 360 [12] using a platform called AutoSDA [13] that enables the automatic design of structural steel frames in addition to evaluation of a given design by users.

Four compartments within the frames are selected in each model, and following some earthquake motions, the temperature rise is initiated for those elements inside the compartment. Ground motions are selected and scaled based on the expected seismic hazard for the region where the structure is supposedly designed. Base-isolated frames have relatively lower drift demands compared to fixed-base frames. Also, residual drift after the fire event is relatively low for base-isolated frames. Parameters for three-parameter log-normal distribution regarding some structural demands, such as drift, maximum moment on the elements of the fire compartment, and axial force on the compartment beam are also given.

## 2. Structural frames

Two base-isolated and fixed-base structural moment resisting frames are designed following the requirements given in ASCE/SEI 7-16 standard. These structural frames differ in terms of floors, and 3 and 4-story buildings are considered for the design of the frames. All archetype frame models consist of the perimeter lateral force resisting systems of a building with a plan dimension of 36.58 m×36.58 m and 4 bays in each direction. All floors have the same height of 3.048 m. Fig. 1 shows a typical representation of each building plan for both fixed-base and base-isolated buildings. There is two lateral force resisting systems in each direction, and earthquake loads are resisted only with these two frames in each principal direction while interior frames are considered gravity systems. Dead and live floor loads are 5.20 kN/m<sup>2</sup> and 2.4 kN/m<sup>2</sup>, respectively, while the roof dead load is considered to be 3.23 kN/m<sup>2</sup> and the live load is the same as floor loads. These values are calculated based on previously designed moment-resisting frames [13–16] and include different loads such as exterior cladding, partition loads, metal deck, etc. Typical floor weights are 7045.98 kN (same for the base level for isolated structures) and the roof weight of the structures is 4323.67 kN.

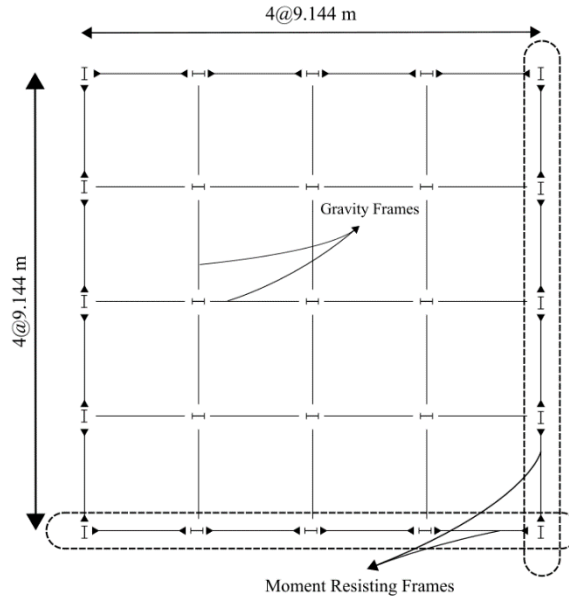


**Fig. 1.** Plan of 4-story building

Buildings are all assumed to be located in San Francisco on a soil type of C, and seismic parameters of the location are given as 1.5 for acceleration parameter at a short period,  $S_s$ , and 0.6 for acceleration parameter at the period of 1-second,  $S_1$ , long period transition,  $T_L$ , is 12.0 seconds [17] for 5%-damped and 2% probability of exceedance in fifty years. All frames are designed based on the minimum drift requirement of ASCE/SEI 7-16. For fixed-base structures, the response modification parameter,  $R$ , is 8, deflection amplification factor  $C_d$  is 5.5, and overstrength factor  $\Omega_0$  is 3. For base-isolated structures  $R_f$  is considered as one and  $C_d$  is taken as equal to  $R_f$ . The design of fixed-base structural frames is carried out with a computational platform that utilizes some optimization technique to decide on steel members to be used in the farming systems based on seismic parameters, geometry, and expected loads on the building [13]. This platform evaluates lateral force resisting the frame's response and optimizes structural members to meet the drift requirement of ASCE/SEI 7-16 [11], in addition to other specifications regarding the steel member to be used in the frame such as beam-column connection criteria, ductile member requirement, and shear and flexural capacities of beam-column connections, and the demand-to-capacity ratio of the members for the relevant standards. [11, 12, 18, 19]. In addition to the design of a structure, this open-source platform [13] is also able to evaluate the adequacy of a given member of a frame system in terms of capacity, connection, etc.

Base-isolated frames are designed based on Chapter 17 of ASCE/SEI 7-16 and drift limitations are checked based on the distributed base shear as per ASCE/SEI 7-16 for the double friction pendulum system shown in Fig. 2. The effective radius of curvature of each sliding surface is 2.12 m, and upper bound (UB) and lower bound (LB) properties are also given for these surfaces, which are decided based on previous studies [16, 20]. In the design phase of base-isolated structures, first, the equivalent lateral force (ELF) procedure is applied to obtain base displacement, damping ratio, base shear, and distributed lateral forces in each floor level, and drift ratios are determined with an iterative process until the drift requirement of ASCE/SEI 7-16 is satisfied for each frame. Then, nonlinear time history analyses are performed in OpenSees [21] to see if the drift ratios are acceptable in terms of seismic design. For the last design step, connection and capacity ratios of base-isolated frames are checked by the AutoSDA platform, and if all requirements are satisfied, final member sizes are decided.

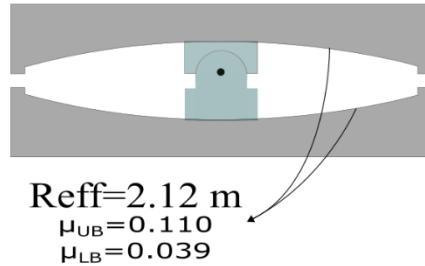


**Fig. 2.** Friction Pendulum system used in analyses

Seven ground motions from Pacific Earthquake Engineering Research Center (PEER) website (<https://ngawest2.berkeley.edu/>) are selected and scaled as per ASCE/SEI 7-16 requirements considering the effective period of isolator for upper and lower bound properties. Table 1 shows ground motions used in nonlinear time history analyses (NTHA) with the record sequence number (RSN) of the PEER website [22]. In this table  $V_s$  is the average shear wave velocity on the upper 30m of the soil, and  $SF$  is the scale factor used for matching spectrum. Fig. 3 illustrates the spectrum of each scaled motion, target spectrum, and mean spectrum in addition to the period range considered for scaling of records to analyze base-isolated structures under upper and lower bound properties. The period range of scaling is decided based on the ASCE/SEI 7-16 requirement. Table 2 shows design values of base shear and drift ratios of each base-isolated frame for upper bound (UB) and lower bound (LB) isolator properties. Those values of shear forces are per frame in the direction considered. The effective period of the isolated structures with upper and lower bound properties are 2.59 sec and 3.64 sec, respectively, and isolator displacements are 303.27 mm and 572.00 mm for the same properties. Member sizes of each frame are given in Table 3. Fig. 4 shows mode shapes and period of vibration of fixed-base frames in the first three modes.

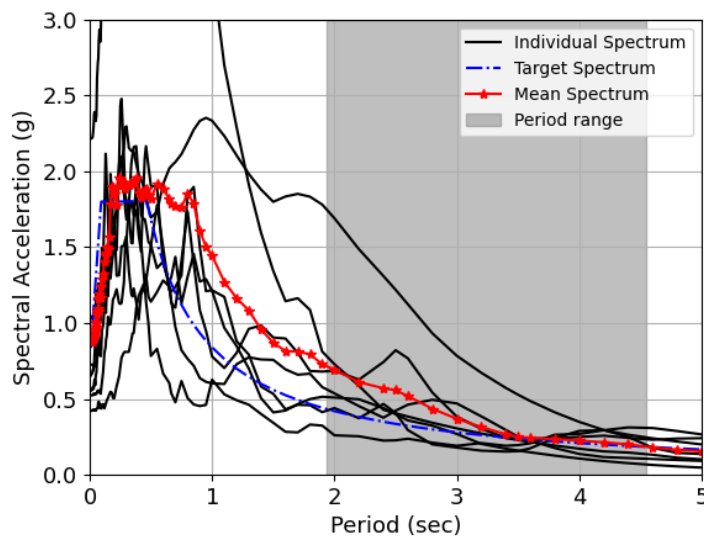
OpenSees model of 4 story base-isolated and fixed-base frames in addition to computational elements used for modeling are shown in Fig. 5. This figure also shows four compartments that are considered fire locations within the structure, and corresponding numbering. For each compartment, beam and two columns elements are exposed to rising temperature considering a time history given in Fig. 6 which is selected based on the relevant literature considering the probabilistic evaluation of fire temperature curves [23–25] and shows the assumed temperature on the surface of corresponding structural elements. Time history and feature of fire curve for rising temperature and cooling part are considered based on the study [26].

Concentrated plastic hinges along the elastic beam-column elements are used to model the nonlinear behavior of the frame elements. Hinges are defined using nonlinear rotational spring with hysteretic behavior [27, 28] and parameters of the model are defined by the studies [15, 28–30]. The hysteric behavior of these springs is controlled by four modes of deterioration. Stiffness, post-capping stiffens, strength, and reloading and unloading stiffness deterioration modes can be captured by the hysteric behavior of the spring elements at joints. Properties of rotational springs to represent plastic hinges are determined based on the beam and column sections. Panel zone elements are utilized to represent shear behavior in the region, and there is a shear spring at the joints.

AutoSDA [13] platform can perform all these calculations regarding the determination of springs parameters, and construction of the nonlinear model of the frames for fixed-base structures. Some procedures given in [13] are also used for modeling base-isolated frames.

**Table 1.** Earthquake ground motion and scale factor for performing nonlinear time history analysis

RSN	Event	Station	Scale Factors	Vs30 (m/s)	Mag	Rrup	Comp
6	Imperial Valley-02	El Centro Array #9	2.58	213.44	6.95	6.09	ELC180
292	Irpinia, Italy-01	Sturno (STN)	2.44	382	6.9	10.84	STU000
821	Erzican, Turkey	Erzincan	2.66	352.05	6.69	4.38	ERX-EW
1004	Northridge-01	LA - Sepulveda VA Hospital	2.94	380.06	6.69	8.44	SPV270
1121	Kobe, Japan	Yae	2.66	256	6.9	27.77	YAE000
6952	Darfield, New Zealand	Papanui High School	2.49	263.2	7	18.73	PPHSS33W
8160	El Mayor-Cucapah, Mexico	El Centro Array #4	2.65	208.91	7.2	35.46	E04090

**Fig. 3.** Spectra of selected and scaled ground motions for base-isolated frames**Table 2.** Design values of base shear ratio<sup>1</sup> and base displacement of each base-isolated frames

Isolator Property	Frame Type	ELF		NTHA	
		F/W <sup>1</sup>	Base Disp. (m)	F/W <sup>1</sup>	Base Disp. (m)
UB	3 Story	0.181	0.20	0.153	0.32
	4 Story	0.182	0.21	0.203	0.28
LB	3 Story	0.173	0.42	0.155	0.41
	4 Story	0.174	0.48	0.175	0.48

<sup>1</sup> Base Shear is given for only the frame considered

Table 3. Beam and column sections of each frame

Frame Type	Floor	Exterior Column	Interior Column	Beam
3-story isolated	Base	NA	NA	W21×147
	1	W24×306	W27×307	W21×147
	2	W24×176	W27×307	W18×175
	Roof	W21×68	W21×93	W18×46
3-story fixed	1	W24×306	W27×336	W21×147
	2	W24×306	W27×336	W21×147
	Roof	W21×68	W21×93	W18×46
4-story isolated	Base	NA	NA	W24×131
	1	W27×235	W27×307	W24×131
	2	W27×235	W27×307	W24×131
	3	W24×162	W24×162	W21×68
4-story fixed	1	W30×261	W30×357	W24×162
	2	W30×261	W30×357	W24×162
	3	W27×102	W24×162	W21×68
	Roof	W27×102	W24×162	W21×68

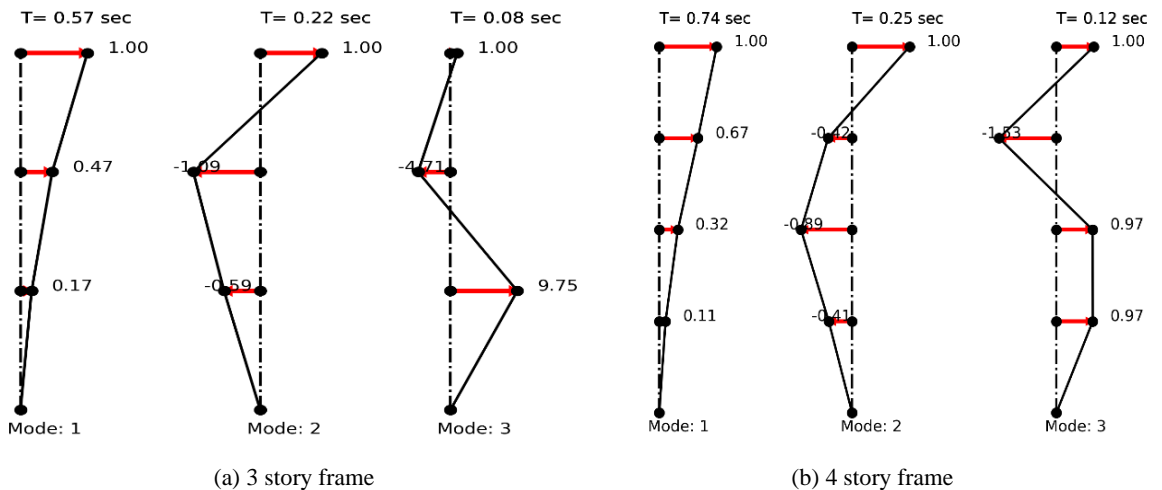
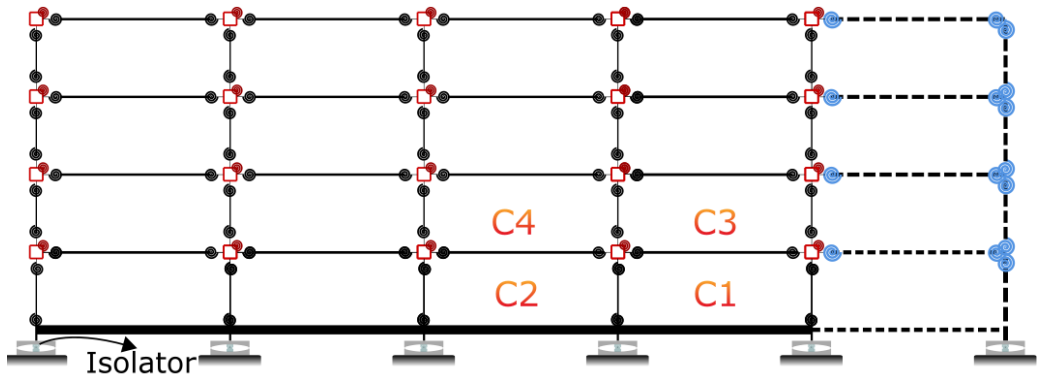
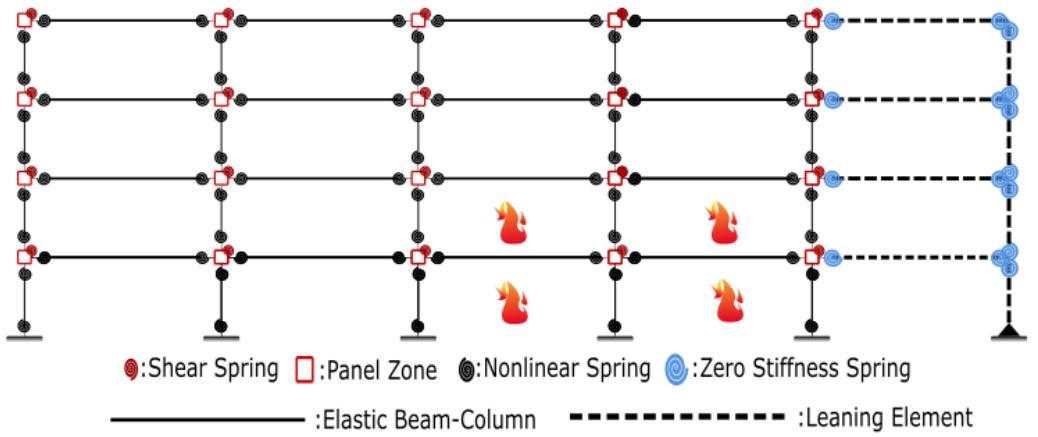


Fig. 4. Mode shape and period of vibration of fixed-base frames



(a) Base-isolated frame



(b) Fixed-base frame

**Fig. 5.** Location of fire compartments, and elements in base-isolated and fixed-base frames

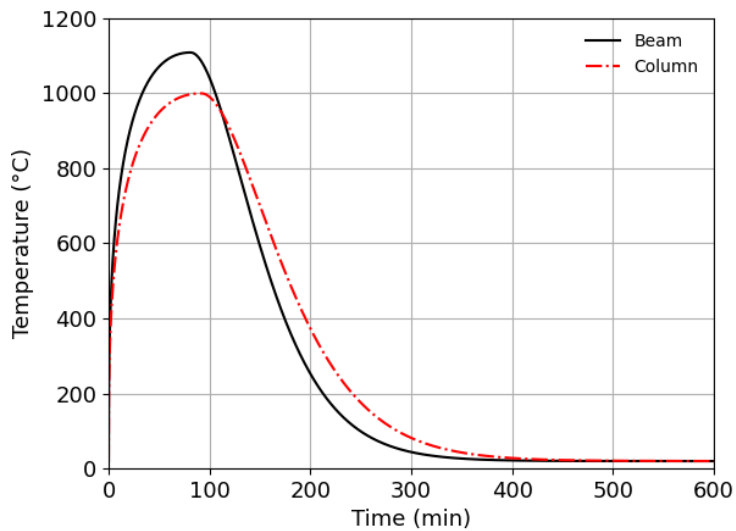


**Fig. 6.** Temperature history for beams and columns

Leaning columns are defined as next-to-moment resisting frames with relatively axially rigid elements with zero rotational spring utilized on each joint in the leaning system so, these elements do not have any rotational resistance but axial rigidity. Point loads on top of each column are assigned considering the half of the load on gravity frames and moment resisting frames to take into account the effect of the gravity framing system, hence, it is considered implicitly in the models. Loads on the moment-resisting frame are subtracted from half of the loads on the gravity frame part of the building to calculate point loads on top of the leaning columns.

Floor leaning columns have a load of 2942.5 kN, roof leaning columns have a load of 1921.63 kN on top of the columns, and floor and roof beams have distributed load of 28.02 kN/m and 18.21 kN/m, respectively which includes the portion of dead and live loads. Since there are two moment-resisting frames in each direction, half of the total weight on each floor is considered for nonlinear modeling. This weight is assigned to each node on floor levels considering lumped mass assumption.

Rotational springs and those elastic elements used for modeling beams and columns in OpenSees are not able to capture thermal effect and respond accordingly. So, for modeling of fire exposed frame members, those elements are replaced with the *dispBeamColumnThermal* elements in OpenSees, which is a fiber-based representation of non-linear structural components based on distributed plasticity. In those thermal elements, there are nine points along with the height where users can define temperature-time history for a thermal loading as input in OpenSees [23, 24, 31]. With strain-based formulation, these elements can capture the behavior of structures in case of a fire event followed by earthquake shaking. After ground-shaking structural elements already have some residual deformation, so this condition has to be preserved at the beginning of thermal loading. A computational model of steel material named *Steel01Thermal* can consider this effect and makes a transition from earthquake to fire analyses smoothly preserving the integrity of the system [23]. This thermal material is based on the strain behavior rather than the stress and can capture strain reversals within a section, which occurs mainly in the cooling part and has an impact on the total response of elements and structural system.

### 3. Selection of ground motions

Ground motions are selected based on the conditional spectrum (CS) approach that links expected seismic hazard on-site to the ground motions that will be used to perform nonlinear time history analyses for a given structural system [32–34]. Unlike a uniform hazard spectrum in which all points in the spectrum have the same probability of exceedance, and which is constructed using the annual frequency of exceedance rate given in seismic hazard curves, the CS approach focuses on a point in the spectrum, which is conditioning period. For the frames in this study seismic hazard curves are depicted in Fig. 7 as obtained from [35]. In the CS approach, results of probabilistic seismic hazard analysis that calculates magnitude, distance, and spectral shape parameters for different earthquake scenarios around the site for a given return period, soil type, spectral period, etc. are used, and those results are given as inputs to ground motion prediction equations that give a mean value of spectral acceleration and standard deviation. The CS constructs the mean value of spectral acceleration based on the ground motion prediction equation, and the effect of spectral shape is an indication of the difference between spectra of selected motion and the mean predicted spectra by a ground motion prediction model that is suitable for the considered site. The probability distribution of log spectral acceleration that is conditioned on a spectral value for a given conditioning period involves in conditional spectrum approach and considers the variability in spectral values at another period as well. Selection and scaling of ground motions are performed based on [36] with the codes given in [37]. All ground motions used in the nonlinear time history analyses are obtained from Pacific Earthquake Engineering Research Center's website [22].

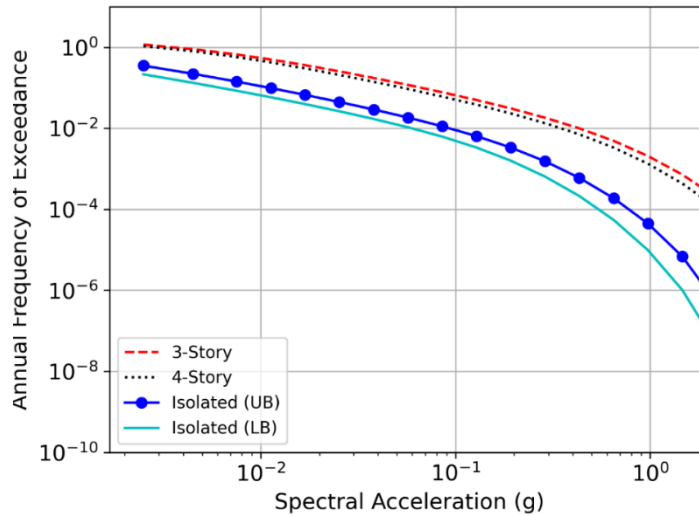


Fig. 7. Seismic hazard curves for all frames

In this study, soil type is considered as C with the classification of ASCE/SEI 7-16 [11] which is also considered in the design phase of the computational models, and there are ten different return periods of earthquakes for the selection of seismic events: 475, 1425, 2475, 3425, 4375, 5325, 6275, 7225, 8175 and 10000 years. Events that have smaller return periods than 475 years are considered not to have gotten ignition initiated within the building since it is already a design base earthquake. In the conditional spectrum method, all spectra are conditioned at a specific structural period. For 3- and 4-story frames this conditioning period is selected as the first natural period of vibration of the 2D models shown in Fig. 4. For the base-isolated frames this selection is based on the effective period of vibration for upper and lower bound properties which are calculated as 2.59 and 3.64 sec in the design phase, respectively.

At each intensity level, five ground motion pairs are selected and scaled, and the matching of these events is calculated depending on the rotD50 spectra, which considers the median value of spectral acceleration in a series of rotated ground motion pairs [38]. Since there are five different events in each intensity level, and there are two records for each pair, a total of a-hundred ground motions are selected for each frame. For each pair of an event, the same scale factors are used and the vertical component of earthquake records are not considered in this study. Fig. 8 shows spectra of selected and scaled ground motions conditioned at the period of 2.59 sec for base-isolated frames with upper bound isolator properties, where the spectrum is conditioned at the period of interest for the frame considered.

#### 4. Post-earthquake fire analyses

Before running any nonlinear time history analyses to simulate earthquakes, there have to be heat transfer analyses conducted so that the proper temperature distribution within the steel section can be applied after ground shaking. The temperature history given in Fig. 6 is assumed to heat beam and column surface of elements in the fire compartment of interest. So, heat transfer analyses are required to obtain temperature-time histories within the section, and the temperature distribution of each column and beam depending on time. For this purpose, heat transfer analyses are performed for each section in those four compartments for each frame with corresponding elements [39,40] considering that there is a unit concrete block on top of the beam. The computational model used for the heat transfer within the W-steel sections considers lumped assumption of properties in three locations within the section and gives the temperature at the center of the web and flanges as given in Fig. 9.

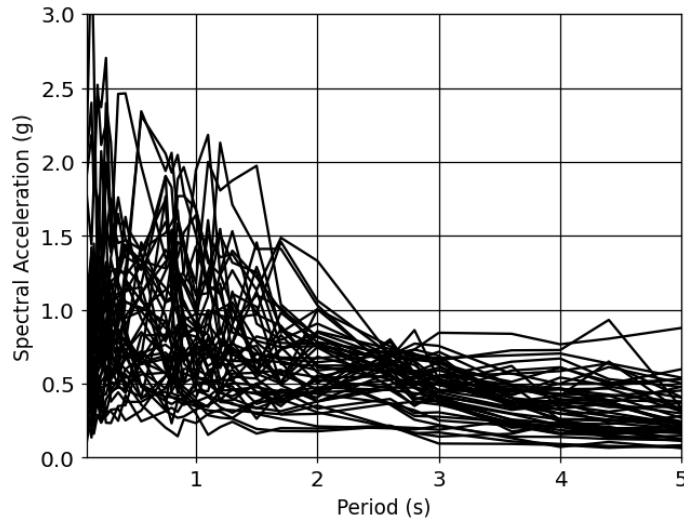


Fig. 8. Spectra for isolated structures with upper bound properties

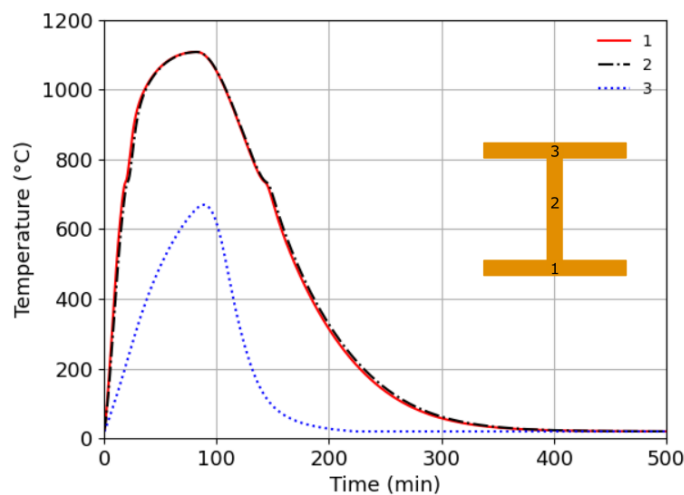


Fig. 9. Temperature distribution on web and flanges of W18X46 beam section

However, in OpenSees, there are nine points selected to define temperature history for any given section, so results of calculation in heat transfer analysis are interpolated throughout the depth so that input values are in conjunction with the definition in the software. This is also important since different temperature values within the same section cause uneven stress distribution, which is also the case in a fire event. Structural members are assumed to have no fire protection on the surface and the building is considered not to have fire sprinkler-like systems equipment. Temperature values on these nine locations with respect to time are recorded and saved in a file to be used in the fire analyses. OpenSees can read these files and apply temperature on the sections to the defined points. Each section is divided into uniform nine pieces to apply temperature history.

All structural frames are analyzed under an a-hundred ground motion that is selected and scaled using the Conditional Spectrum approach at first. Ground motions are padded with zero for ten more seconds so that all structures are at rest before temperature increases in sections to simulate ignition of the fire. At the end of earthquake analyses, the condition of the structures and structural demands on the element is preserved

hence, there is no data loss during the transition from earthquake to fire analyses. This is an important point because these two analyses are run on the same platform with the material and loading patterns available in OpenSees software. In earthquake analyses, all nodes at floor levels are restrained to move together, however, under fire, concrete on top of the beam cannot sustain this behavior due to cracking at the early stages of temperature rise [23]. Hence, after ground shaking, two end nodes of the beam in the compartments where the fire event is assumed to occur are released to capture cracking behavior and respond accordingly, while other nodes still have to restrain and move together in the horizontal direction with the adjacent floor nodes. Since there is no restraint on top of columns in the fire compartment, these nodes can move independently from others on the floor level. Hence, drift values on those floors in a fire event are calculated as the average drift of the two columns exposed to fire since other floor nodes will follow on top of these two. Maximum drift during fire analyses and residual drift at the end of the fire are calculated and recorded for the first two stories in each frame. Each section within the compartments is exposed to temperature increases at nine points on which temperature history is defined beforehand.

## 5. Results

Results of the study are given in terms of drift on floors, moment, and axial force demand in the elements of fire compartments. Maximum drift and other quantities of fixed-base frames during fire after an earthquake shaking, and after this fire event is over are normalized with the same results of base-isolated frames. Hence, the results of these two frame configurations can be compared and the effect of the seismic protective system can be obtained for post-earthquake fire analysis. Also, fire-following-earthquake results in terms of drift demand are normalized with the results of the fire-only event for both isolated and fixed-base frames to reveal how an earthquake affects the drift of structural frames before thermal loading. Analyses are performed in the OpenSees computational platform, which can conduct both fire and earthquake analyses without losing the integrity of the structural system, has been used for fire and simulation of earthquake response of different systems [23, 41–43]. Data obtained at the end of analyses are processed so that robust comparison can be given. Convergence of each analysis is checked in both fire and earthquake simulations, and those that have numerical divergence in either of them are not taken into account. After, some outliers are also removed from the data-set, which is achieved considering only those data that fall between mean minus two standard deviations and mean plus two standard deviations. Table 4 shows results of maximum and residual drift values in the first two floors where fire compartments are assumed to be located in case of a fire-only event. Subscript  $fr$  denotes values during the fire, and  $fr_{Res}$  shows the value of the quantity after the fire event is over. Drift values of fixed-base frames are normalized with the results of base-isolated frames. Engineering demand parameters (EDPs),  $\Delta_1$  and  $\Delta_2$  show drift ratios of the first and second floor, respectively.  $\sigma$ ,  $\mu$  and  $\alpha$  are the shape, scale, and location parameters of three-parameter log-normal distribution, respectively, and those values can be used for the construction of fragility curves for frames considering fire events in four compartments or for the calculation of the probability of non-exceedance of given values of EDP.  $x_{P50}$  values denote normalized EDP that has a fifty percent of probability of exceedance in the case of both upper and lower isolator properties. Drift demands in the first two stories during a fire event are higher for fixed-base structures. The only exemption is the fire in compartment number two of the three-story frame, which has slightly higher drift values for base-isolated structures. Residual drift demands for compartments number one and three have higher values for fixed-base frames. An increase in residual drift demand on the first floor for fixed-base frames is more pronounced if the fire is in compartment number either one or three. Drift during the fire event in compartments number one and three also results in higher values for fixed-base frames on the first floor. Although, some values in Table 4 are lower than one, indicating base-isolated frames have higher drift values compared to fixed ones, in an average sense base-isolated frames have lower drift demands in comparison.

Table 4. Drift demands of fixed-base frames normalized with base-isolated frames results

N	Comp.	EDP	$\sigma_{UB}$	$\mu_{UB}$	$\gamma_{UB}$	$\sigma_{LB}$	$\mu_{LB}$	$\gamma_{LB}$	$x_{p_{50UB}}$	$x_{p_{50LB}}$
3	C1	$\Delta_{1fr}$	0.744	0.975	0.255	0.739	0.980	0.260	1.23	1.24
		$\Delta_{2fr}$	0.610	0.720	0.762	0.590	0.803	0.924	1.48	1.73
		$\Delta_{1fr_{Res}}$	0.766	0.981	0.216	0.762	0.985	0.220	1.20	1.21
		$\Delta_{2fr_{Res}}$	0.263	-3.664	7.343	0.209	-7.865	13.341	3.68	5.48
	C2	$\Delta_{1fr}$	0.610	0.487	0.370	0.605	0.468	0.351	0.86	0.82
		$\Delta_{2fr}$	1.336	0.530	0.377	1.243	0.416	0.353	0.91	0.77
		$\Delta_{1fr_{Res}}$	0.442	0.454	0.323	0.436	0.436	0.306	0.78	0.74
		$\Delta_{2fr_{Res}}$	0.738	-0.123	0.814	0.725	-0.097	0.647	0.69	0.55
	C3	$\Delta_{1fr}$	1.290	1.060	0.205	0.592	0.875	1.203	1.26	2.08
		$\Delta_{2fr}$	0.735	0.755	0.029	1.078	0.769	0.014	0.78	0.78
		$\Delta_{1fr_{Res}}$	0.409	-0.452	1.906	0.288	-1.462	3.465	1.45	2.00
		$\Delta_{2fr_{Res}}$	0.525	1.162	0.077	0.534	1.182	0.066	1.24	1.25
C4	$\Delta_{1fr}$	0.411	-0.247	2.193	0.365	-0.652	3.396	1.95	2.74	
	$\Delta_{2fr}$	0.489	0.811	0.159	0.876	0.757	0.038	0.97	0.79	
	$\Delta_{1fr_{Res}}$	0.352	-1.175	2.563	0.739	-3.497	19.986	1.39	16.49	
	$\Delta_{2fr_{Res}}$	0.322	0.778	0.177	0.597	0.746	0.040	0.96	0.79	
4	C1	$\Delta_{1fr}$	0.040	-5.370	6.692	0.047	-4.557	5.904	1.32	1.35
		$\Delta_{2fr}$	0.742	0.706	0.405	0.715	0.832	0.551	1.11	1.38
		$\Delta_{1fr_{Res}}$	0.095	-0.499	1.808	0.099	-0.430	1.759	1.31	1.33
		$\Delta_{2fr_{Res}}$	0.390	-0.719	3.342	0.460	-1.496	7.796	2.62	6.30
	C2	$\Delta_{1fr}$	0.581	0.584	0.369	0.578	0.535	0.345	0.95	0.88
		$\Delta_{2fr}$	1.078	0.693	0.862	0.960	0.339	0.487	1.56	0.83
		$\Delta_{1fr_{Res}}$	0.185	-0.710	1.639	0.183	-0.661	1.517	0.93	0.86
		$\Delta_{2fr_{Res}}$	1.062	-0.088	1.579	0.838	-0.094	0.701	1.49	0.61
	C3	$\Delta_{1fr}$	0.349	-0.098	1.195	0.309	-0.249	1.794	1.10	1.55
		$\Delta_{2fr}$	0.294	0.839	0.141	0.288	0.839	0.148	0.98	0.99
		$\Delta_{1fr_{Res}}$	0.108	-2.429	3.374	0.301	-0.918	2.415	0.95	1.50
		$\Delta_{2fr_{Res}}$	0.124	0.823	0.159	0.182	0.893	0.094	0.98	0.99
C4	$\Delta_{1fr}$	0.624	1.077	0.718	0.602	1.571	1.417	1.79	2.99	
	$\Delta_{2fr}$	1.211	0.163	0.136	1.118	0.148	0.142	0.30	0.29	
	$\Delta_{1fr_{Res}}$	0.164	-2.572	5.050	0.638	-2.299	20.458	2.48	18.16	
	$\Delta_{2fr_{Res}}$	0.826	-0.033	0.241	0.820	-0.033	0.230	0.21	0.20	

Table 5. Drift demands of fire-following-earthquake results normalized with the fire-only event

N	Comp.	EDP	$\sigma_{Fixed}$	$\mu_{Fixed}$	$\gamma_{Fixed}$	$\sigma_{Fixed}$	$\mu_{Fixed}$	$\gamma_{Fixed}$	$x_{P_{50}Fixed}$	$x_{P_{50}Iso}$
3	C1	$\Delta_1$	0.753	0.847	0.219	0.117	0.974	0.022	1.07	1.00
		$\Delta_2$	0.566	0.587	0.608	0.215	0.880	0.140	1.19	1.02
		$\Delta_{1Res}$	0.776	0.867	0.188	1.688	0.992	0.005	1.05	1.00
		$\Delta_{2Res}$	0.182	-2.063	3.297	0.008	-6.427	7.411	1.23	0.98
	C2	$\Delta_1$	1.553	0.943	0.105	0.003	-1.040	2.090	1.05	1.05
		$\Delta_2$	1.272	0.955	0.737	0.003	-10.041	11.276	1.69	1.23
		$\Delta_{1Res}$	1.070	0.910	0.087	0.003	-0.954	2.004	1.00	1.05
		$\Delta_{2Res}$	0.740	-0.195	1.370	0.003	-10.545	11.805	1.18	1.26
	C3	$\Delta_1$	2.225	0.999	0.266	0.284	0.842	0.169	1.26	1.01
		$\Delta_2$	1.444	0.979	0.026	1.685	0.996	0.004	1.01	1.00
		$\Delta_{1Res}$	0.770	0.088	1.304	0.009	-7.645	8.643	1.39	1.00
		$\Delta_{2Res}$	1.091	0.978	0.078	1.685	0.995	0.004	1.06	1.00
C4	$\Delta_1$	0.906	0.714	0.398	0.039	-0.228	1.207	1.11	0.98	
	$\Delta_2$	0.855	0.984	0.037	0.005	-1.530	2.706	1.02	1.18	
	$\Delta_{1Res}$	0.278	-1.060	1.988	0.064	0.168	0.806	0.93	0.97	
	$\Delta_{2Res}$	0.599	0.983	0.036	0.005	-1.530	2.706	1.02	1.18	
4	C1	$\Delta_1$	0.479	0.791	0.213	0.188	0.968	0.038	1.00	1.01
		$\Delta_2$	0.714	0.618	0.343	0.054	0.165	0.876	0.96	1.04
		$\Delta_{1Res}$	0.477	0.803	0.193	0.018	0.795	0.211	1.00	1.01
		$\Delta_{2Res}$	0.381	-0.283	1.233	0.007	-14.949	15.977	0.95	1.03
	C2	$\Delta_1$	1.339	0.958	0.077	0.011	0.165	0.919	1.04	1.08
		$\Delta_2$	1.231	0.847	0.705	0.004	-21.920	23.882	1.55	1.96
		$\Delta_{1Res}$	1.004	0.931	0.087	0.008	-0.181	1.265	1.02	1.08
		$\Delta_{2Res}$	0.799	-0.287	1.889	0.005	-23.925	26.220	1.60	2.30
	C3	$\Delta_1$	1.373	0.953	0.110	0.003	-8.483	9.481	1.06	1.00
		$\Delta_2$	0.590	0.965	0.047	0.190	0.980	0.020	1.01	1.00
		$\Delta_{1Res}$	0.219	-0.827	1.849	0.002	-13.417	14.413	1.02	1.00
		$\Delta_{2Res}$	0.207	0.931	0.078	0.181	0.980	0.020	1.01	1.00
C4	$\Delta_1$	1.339	0.958	0.077	0.007	-10.444	11.478	1.04	1.03	
	$\Delta_2$	1.231	0.847	0.705	0.038	0.688	0.373	1.55	1.06	
	$\Delta_{1Res}$	1.004	0.931	0.087	0.037	-2.716	3.711	1.02	1.00	
	$\Delta_{2Res}$	0.799	-0.287	1.889	0.008	-0.701	1.762	1.60	1.06	

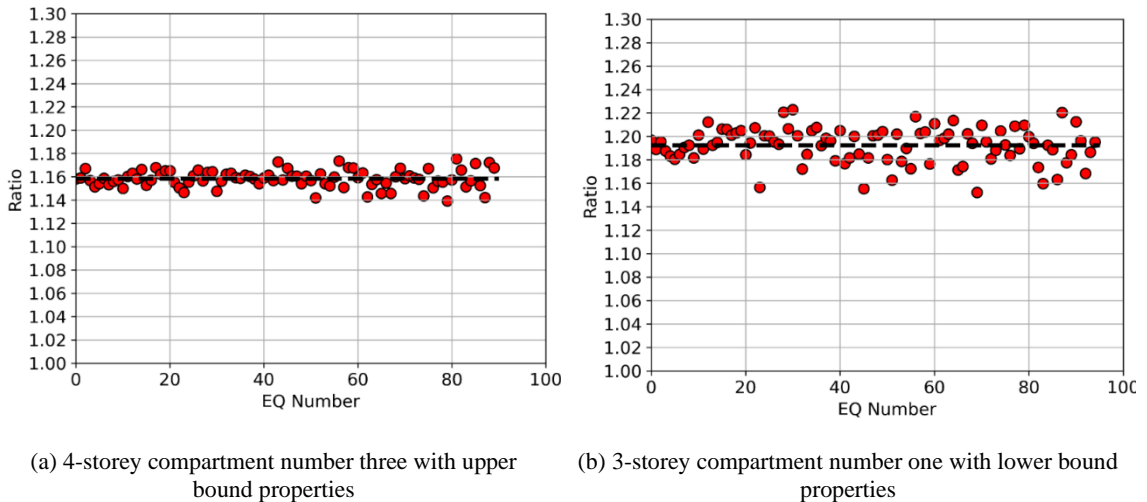


Fig. 10. Normalized maximum normal force in the beam

Also, results of fire-following-earthquake demand are normalized with the results of fire-only events to further understand the behavior and see the response of each frame. Table 5 shows statistical parameters and results of normalized engineering demand parameter (EDP) that has a fifty percent probability of exceedance. Results of base-isolated frame belong to a maximum of upper and lower bound properties in the table. For three-story frames drift demands of fixed-base structures during the fire are higher for almost all compartment fires in the first two stories. Residual drift demand in the compartment one and three is lower for base-isolated frames, while the results of both frames are close for other compartments. In the case of a four-story frame, fire in second-floor compartments of fixed-base frame increased both maximum and residual drift demand as compared to other fire locations if frames had pre-fire earthquakes. On the other hand, base-isolated frames have a more pronounced drift demand in case of a post-earthquake fire event on the first floor of these buildings. Table 5 in conjunction with the 4 shows the effectiveness of the base isolation system in case of a fire after ground shaking. Although there is no significant difference in the drift demand of base-isolated and fixed-based frames for four-story structures as given in Table 5, demands of fixed-base configuration are higher than base-isolated frames as given in Table 4.

Maximum, minimum and residual force and moment demand of elements within the fire compartment is also compared to understand how fire increases or decreases the demands of the elements. Fig. 10 shows the ratio of maximum force in the beams of a fixed-base structure normalized with the same element in the base-isolated frame for both upper and lower bound properties of four and three-story frames, respectively, for fire events in third and first compartments. The average increase in maximum beam force of fixed-base frame in both comparisons is around 16% and 19%, respectively.

Statistical parameters for normalized maximum, minimum and residual normal force of fixed-base frame are given in Table 6 which shows maximum and minimum axial force on beam during fire after an earthquake, and the residual force after the fire event, which are denoted by  $N_{max}$ ,  $N_{min}$ , and  $N_{Res}$ .

Force demand in fixed-base structures is higher as compared to base-isolated frames. This increase is more pronounced for four-story buildings in case of a fire in compartments number two and four. The increase, however, in three-story configurations is not as much as in four-story structures. The results for three-story frames are close to each other and there is no significant increase for different fire compartments. Residual and minimum force ratios in the beams are similar, and maximum force is slightly higher for almost all cases. This decrease in normal force for the heated beam of base-isolated structure is important since axial force will push the joints and force columns to deform laterally in case of a temperature increase. Once, the

maximum temperature value is reached there will be strain reversal in the beam element and this will pull the joint and deform columns in the reverse direction in the cooling phase of the fire. So, if the force increase and decrease are reduced, this action might have less detrimental to column behavior and story drift demand.

In addition to the normal force on the beam, moments in the columns and beam elements are also investigated. Figs. 11a and 11b show the cumulative distribution function plot of normalized maximum moments of the heated beam in case of fire in compartment number three for isolated frames with lower and upper bound properties. The average increase in the beam moment for these two types of configuration is around 17% and 18%.

Normalized maximum moment of beam and columns for post-earthquake fire in each compartment are given in Table 7, where  $Col_L$  and  $Col_R$  show the left and right column in each fire compartment. For a four-story frame, moment demand is higher for fixed-based configuration in almost all compartments in both beams and column elements. The average increase in the beam is around 20%, while this value is higher for the right column. Although there is a decrease for the left column in compartment number one, in other compartments it is also under some moment increase as compared to base-isolated structures. For three-story buildings, right columns have an increase in moment demand around 10-15% in compartments number one and there, while there is some demand increase in compartments number two and four for base-isolated structures in three-story buildings.

Table 6. Statistical parameters of normalized axial force demand in beams

N	Comp.	Quantity	$\sigma_{UB}$	$\mu_{UB}$	$\gamma_{UB}$	$\sigma_{LB}$	$\mu_{LB}$	$\gamma_{LB}$	$x_{P_{50UB}}$	$x_{P_{50LB}}$
3	C1	$N_{max}$	0.004	-2.305	3.488	0.005	-1.723	2.915	1.18	1.19
		$N_{res}$	0.005	0.142	0.944	0.003	-0.286	1.371	1.09	1.09
		$N_{min}$	0.006	0.322	0.763	0.006	0.350	0.734	1.08	1.08
	C2	$N_{max}$	0.006	-0.049	1.121	0.012	0.477	0.605	1.07	1.08
		$N_{res}$	0.267	1.039	0.009	0.244	1.041	0.006	1.05	1.05
		$N_{min}$	0.252	1.037	0.009	0.187	1.037	0.008	1.05	1.05
	C3	$N_{max}$	0.146	0.924	0.067	0.011	-0.096	1.096	0.99	1.00
		$N_{res}$	0.349	1.004	0.015	0.392	1.015	0.013	1.02	1.03
		$N_{min}$	0.311	1.000	0.018	0.343	1.012	0.013	1.02	1.03
	C4	$N_{max}$	0.025	-0.296	1.089	0.009	-1.154	2.170	0.79	1.02
		$N_{res}$	0.198	0.973	0.070	0.008	0.219	0.946	1.04	1.16
		$N_{min}$	0.045	0.521	0.500	0.007	0.196	0.969	1.02	1.17
4	C1	$N_{max}$	0.013	0.602	0.731	0.007	-0.339	1.692	1.33	1.35
		$N_{res}$	0.004	-0.755	1.947	0.002	-2.796	3.988	1.19	1.19
		$N_{min}$	0.006	-0.264	1.456	0.004	-1.174	2.367	1.19	1.19
	C2	$N_{max}$	0.015	0.918	0.375	0.009	0.713	0.604	1.29	1.32
		$N_{res}$	0.049	1.250	0.029	1.491	1.278	0.002	1.28	1.28
		$N_{min}$	1.496	1.276	0.003	1.491	1.277	0.002	1.28	1.28
	C3	$N_{max}$	0.008	0.232	0.927	0.016	0.725	0.438	1.16	1.16
		$N_{res}$	0.313	1.139	0.014	0.234	1.145	0.021	1.15	1.17
		$N_{min}$	0.317	1.142	0.014	0.243	1.148	0.020	1.16	1.17
	C4	$N_{max}$	2.276	1.482	0.010	0.016	0.969	0.560	1.49	1.53
		$N_{res}$	0.017	0.972	0.412	0.087	1.367	0.040	1.38	1.41
		$N_{min}$	0.057	1.249	0.128	0.028	1.258	0.145	1.38	1.40

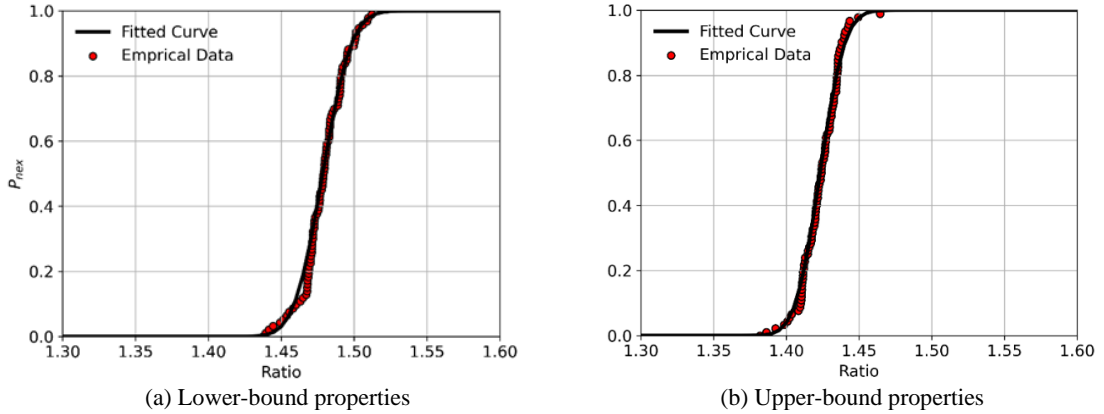


**Fig. 11.** Normalized maximum moment of four-story frames in case of fire in compartment number three

**Table 7.** Statistical parameters of normalized moment demand in beam and columns for different compartments

N	Comp.	Element	$\sigma_{UB}$	$\mu_{UB}$	$\gamma_{UB}$	$\sigma_{LB}$	$\mu_{LB}$	$\gamma_{LB}$	$x_{P_{50UB}}$	$x_{P_{50LB}}$
3	C1	Beam	0.605	0.970	0.035	0.621	0.985	0.031	1.01	1.02
		Col <sub>L</sub>	0.009	-0.973	1.652	0.010	-0.813	1.485	0.68	0.67
		Col <sub>R</sub>	0.179	1.098	0.080	0.119	1.059	0.126	1.18	1.18
	C2	Beam	0.113	0.899	0.099	0.567	0.988	0.011	1.00	1.00
		Col <sub>L</sub>	0.010	-0.831	1.885	0.004	-3.603	4.654	1.05	1.05
		Col <sub>R</sub>	0.010	-3.404	4.300	0.007	-5.292	6.172	0.90	0.88
	C3	Beam	0.166	0.918	0.038	1.697	0.970	0.006	0.96	0.98
		Col <sub>L</sub>	0.011	-1.448	2.346	0.007	-2.276	3.086	0.90	0.81
		Col <sub>R</sub>	0.287	1.056	0.038	0.216	1.051	0.054	1.09	1.11
	C4	Beam	0.082	0.678	0.339	0.016	-0.908	1.830	1.02	0.92
		Col <sub>L</sub>	0.008	-4.737	6.539	0.155	0.964	0.097	1.80	1.06
		Col <sub>R</sub>	0.023	0.192	0.579	0.014	-0.063	0.910	0.77	0.85
4	C1	Beam	1.433	1.211	0.011	0.461	1.203	0.017	1.22	1.22
		Col <sub>L</sub>	0.478	0.777	0.058	0.512	0.758	0.050	0.83	0.81
		Col <sub>R</sub>	0.004	-2.103	3.484	0.005	-1.230	2.629	1.38	1.40
	C2	Beam	1.503	1.221	0.009	1.502	1.222	0.008	1.23	1.23
		Col <sub>L</sub>	0.013	-0.029	1.434	0.009	-0.640	2.070	1.41	1.43
		Col <sub>R</sub>	0.013	-1.151	2.412	0.011	-1.251	2.464	1.26	1.21
	C3	Beam	0.009	-0.028	1.452	0.011	0.096	1.383	1.42	1.48
		Col <sub>L</sub>	0.092	0.799	0.254	0.018	-0.376	1.308	1.05	0.93
		Col <sub>R</sub>	0.871	1.228	0.005	0.470	1.231	0.018	1.23	1.25
	C4	Beam	0.060	1.066	0.114	0.237	1.140	0.060	1.18	1.20
		Col <sub>L</sub>	0.072	1.073	0.281	0.007	-1.244	2.649	1.35	1.41
		Col <sub>R</sub>	0.058	0.786	0.576	0.005	-6.405	7.657	1.36	1.25

## 6. Conclusion

In this study, the fire performance of three and four-story steel moment-resisting frames with base isolation and fixed-base configuration is investigated. Frames are designed as perimeter lateral force resisting systems of a building as per seismic design requirements of ASCE/SEI 7-16 and some other ANSI/AISC standards. Four different fire compartments are selected on the first two floors of each frame, and heat transfer analyses are performed to determine the temperature-time history of the beams and columns within those compartments, which are used to apply thermal loads on the structural elements. A hundred ground motions are selected and scaled based on the conditional spectrum approach for ten different seismic intensity levels depending on the return periods, and the results of probabilistic seismic hazard analysis for the location are considered.

Each frame is firstly subjected to earthquake shaking, then fire is applied to the structure as temperature increases in the elements of fire compartments while it is under residual demands due to earthquake shaking. Maximum drift ratios during a fire event and drift ratios after thermal loading are over are recorded. Those results of fixed-base frames are normalized with the results of base-isolated structures. Hence, how seismic isolation affects post-earthquake fire performance of three and four-story structures is investigated. Moreover, the drift values of each frame under a fire-only event are also recorded, and the fire-following-earthquake results of frames are normalized with the results of the fire-only event.

Base-isolated frames performed well compared to fixed-base structures in terms of maximum drift demand of frames, which is an important factor in the collapse evaluation of structures. An increase in drift demand of fixed-base structure can reach two as compared to base-isolated frames, and in four-story frames, base isolation efficiency is more pronounced. Residual drift ratios of fixed-base structures are also relatively higher compared to base-isolated frames.

Normalized force on the heated beam and moments in the columns are also compared. Thermal loading in the beam of fixed-base frames resulted in almost 20% higher normal force demand. Maximum moments in the beam during fire events are almost the same for three-story frames, however, there is an increase in four-story buildings.

The results of the study are valid for 2D frames and fire-temperature history given in the study. The findings of the study can give some ideas about the possible effect on the post-earthquake fire of base-isolated structures, and the efficiency of seismically isolated frames in comparison to fixed frames. More fire temperature curves and structural frames will reveal behavior and performance comparison in detail. Although lower two stories are considered for the location of fire events, other compartments can be evaluated to estimate and have an idea about the drift, force, and moment demands of the members exposed to thermal loading.

## Declaration of conflicting interests

The author(s) declared no potential conflicts of interest with respect to the research, authorship, and/or publication of this article.

## Acknowledgments

Dr. Shoma Kitayama from the University of Leeds provided comments on the design of base-isolated structural frames. Dr. Xinguan Guan from the University of California, Los Angeles, commented on how to get base-isolated structures evaluated by the AutoSDA platform. The author gratefully acknowledges their valuable comments and help.

## References

- [1] Khorasani NE, Gardoni P, Garlock M (2015) Probabilistic fire analysis: material models and evaluation of steel structural members. *Journal of Structural Engineering* 141(12):04015050.
- [2] Khorasani NE, Garlock ME (2017) Overview of fire following earthquake: Historical events and community responses. *International Journal of Disaster Resilience in the Built Environment* 8(2):158-174.
- [3] Shang J, Tan P, Han J, Zhang Y, Li Y (2022) Performance of seismically isolated buildings with variable friction pendulum bearings under near-fault ground motions. *Journal of Building Engineering* 45:103584.
- [4] Tena-Colunga A, Pérez-Rocha LE, Avilés J, Cordero-Macías C (2015). Seismic isolation of buildings for power stations considering soil-structure interaction effects. *Journal of Building Engineering* 4:21-40.
- [5] Rakicevic Z, Bogdanovic A, Farsangi EN, Sivandi-Pour A (2021) A hybrid seismic isolation system toward more resilient structures: Shaking table experiment and fragility analysis. *Journal of Building Engineering* 38:102194.
- [6] Lee D, Constantinou MC (2018) Combined horizontal-vertical seismic isolation system for high-voltage-power transformers: development, testing and validation. *Bulletin of Earthquake Engineering* 16(9):4273-4296.
- [7] Kitayama S, Cilsalar H (2022) Seismic loss assessment of seismically isolated buildings designed by the procedures of ASCE/SEI 7-16. *Bulletin of Earthquake Engineering* 20(2):1143-1168.
- [8] Sani HP, Gholhaki M, Banazadeh M (2017) Seismic performance assessment of isolated low-rise steel structures based on loss estimation. *Journal of Performance of Constructed Facilities* 31(4):04017028.
- [9] Sayani PJ, Erduran E, Ryan KL (2011) Comparative response assessment of minimally compliant low-rise base-isolated and conventional steel moment-resisting frame buildings. *Journal of Structural Engineering* 137(10):1118-1131.
- [10] Cutfield M, Ryan K, Ma Q (2016) Comparative life cycle analysis of conventional and base-isolated buildings. *Earthquake Spectra* 32(1):323-343.
- [11] ASCE/SEI 7 (2017) Minimum Design Loads for Buildings and Other Structures. American Society of Civil Engineers, VA, USA.
- [12] American Institute for Steel Construction (AISC) (2016) Specification for Structural Steel Buildings, ANSI/AISC 360. American Institute for Steel Construction Chicago, IL, USA.
- [13] Guan X, Burton H, Sabol T (2020) Python-based computational platform to automate seismic design, nonlinear structural model construction and analysis of steel moment resisting frames. *Engineering Structures* 224:111199.
- [14] Guan M EERI X, Burton M EERI H, Shokrabadi M (2021) A database of seismic designs, nonlinear models, and seismic responses for steel moment-resisting frame buildings. *Earthquake Spectra* 37(2):1199-1222.
- [15] Lignos D (2008) Sidesway Collapse of Deteriorating Structural Systems under Seismic Excitations. Ph.D. Dissertation. Stanford University.
- [16] Kitayama S, Constantinou MC (2019) Probabilistic seismic performance assessment of seismically isolated buildings designed by the procedures of ASCE/SEI 7 and other enhanced criteria. *Engineering Structures* 179:566-582.
- [17] USGS. United States Geological Survey (2021) <https://earthquake.usgs.gov/nshmp-haz-ws/hazard> (accessed: November 2021).
- [18] American Institute for Steel Construction (AISC) (2016) Seismic Provisions for Structural Steel Buildings, ANSI/AISC 341-16. American Institute for Steel Construction Chicago, IL, USA.
- [19] American Institute of Steel Construction (AISC) (2016) Prequalified Connections for Special and Intermediate Steel Moment Frames for Seismic Applications, ANSI/AISC 358-16.
- [20] Federal Emergency Management Agency (FEMA) (2015) NEHRP Recommended Seismic Provisions: Design Examples. FEMA P-1051. Washington DC, USA.
- [21] McKenna FT (1997) Object-Oriented Finite Element Programming: Frameworks for Analysis, Algorithms and Parallel Computing. Ph.D. Dissertation, Department of Civil and Environmental Engineering, University of California, Berkeley.
- [22] PEER. Pacific Earthquake Engineering Research Center (2020) <https://ngawest2.berkeley.edu/> (accessed: January 2020).
- [23] Khorasani NE, Garlock ME, Quiel SE (2015) Modeling steel structures in OpenSees: Enhancements for fire and multi-hazard probabilistic analyses. *Computers & Structures* 157:218-231.

- [24] Khorasani NE (2015) A Probabilistic Framework for Multi-Hazard Evaluations of Buildings and Communities Subject to Fire and Earthquake Scenarios. Ph.D. Dissertation, Princeton University.
- [25] Khorasani NE, Garlock M, Gardoni P (2014) Fire load: Survey data, recent standards, and probabilistic models for office buildings. *Engineering Structures* 58:152–165.
- [26] Ma Z, Mäkeläinen, P (2000) Parametric temperature–time curves of medium compartment fires for structural design. *Fire Safety Journal* 34(4):361–375.
- [27] Ibarra LF, Krawinkler H (2005) Global collapse of frame structures under seismic excitations. John A. Blume Earthquake Engineering Center Technical Report 152. Stanford Digital Repository. Available at <http://purl.stanford.edu/dj885ym2486>.
- [28] Ibarra LF, Medina RA, Krawinkler H (2005) Hysteretic models that incorporate strength and stiffness deterioration. *Earthquake Engineering & Structural Dynamics* 34(12):1489–1511.
- [29] Lignos DG, Krawinkler H (2011) Deterioration modeling of steel components in support of collapse prediction of steel moment frames under earthquake loading. *Journal of Structural Engineering* 137(11):1291–1302.
- [30] Lignos DG, Hartloper AR, Elkady A, Deierlein GG, Hamburger R (2019) Proposed updates to the ASCE 41 nonlinear modeling parameters for wide-flange steel columns in support of performance-based seismic engineering. *Journal of Structural Engineering* 145(9):04019083.
- [31] Lange D, Roben C, Usmani A (2012) Tall building collapse mechanisms initiated by fire: Mechanisms and design methodology. *Engineering Structures* 36:90–103.
- [32] Ha SJ, Han SW (2016) An efficient method for selecting and scaling ground motions matching target response spectrum mean and variance. *Earthquake Engineering & Structural Dynamics* 45(8):1381–1387.
- [33] Lin T, Harmsen SC, Baker JW, Luco N (2013) Conditional spectrum computation incorporating multiple causal earthquakes and ground-motion prediction models. *Bulletin of the Seismological Society of America* 103(2A):1103–1116.
- [34] Jayaram N, Lin T, Baker JW (2011) A computationally efficient ground-motion selection algorithm for matching a target response spectrum mean and variance. *Earthquake Spectra* 27(3):797–815.
- [35] USGS. Unified Hazard Tool (2021) <https://earthquake.usgs.gov/hazards/interactive/> (accessed: April 2021)
- [36] Baker JW, Lee C (2018) An improved algorithm for selecting ground motions to match a conditional spectrum. *Journal of Earthquake Engineering* 22(4):708–723.
- [37] Baker J (2021) Conditional spectrum ground motion selection. Available at [https://github.com/bakerjw/CS\\_Selection](https://github.com/bakerjw/CS_Selection) (accessed: November 25, 2021).
- [38] Boore D (2010). Orientation-independent, nongeometric-mean measures of seismic intensity from two horizontal components of motion. *Bulletin of the Seismological Society of America* 100(4):1830–1835.
- [39] Quiel SE, Garlock ME (2010) Closed-form prediction of the thermal and structural response of a perimeter column in a fire. *The Open Construction and Building Technology Journal* 4:64–78.
- [40] Ghojel JI, Wong M (2005) Three-sided heating of I-beams in composite construction exposed to fire. *Journal of Constructional Steel Research* 61(6):834–844.
- [41] Xing Z, Zhang J, Chen H (2022) Research on fire resistance and material model development of CLT components based on OpenSees. *Journal of Building Engineering* 45:103670.
- [42] Usmani A, Zhang J, Jiang J, Jiang Y, May I (2012) Using OpenSees for structures in fire. *Journal of Structural Fire Engineering* 3(1):57–70.
- [43] Jiang J, Li GQ, Usmani A (2014) Progressive collapse mechanisms of steel frames exposed to fire. *Advances in Structural Engineering* 17(3):381–398.